

www.acsami.org Research Article

Development of an ALD-Pt@SWCNT/Graphene 3D Nanohybrid Architecture for Hydrogen Sensing

Bo Liu,* Mohammed Alamri, Michael Walsh, Jennifer L. Doolin, Cindy L. Berrie, and Judy Z. Wu*



Cite This: ACS Appl. Mater. Interfaces 2020, 12, 53115-53124



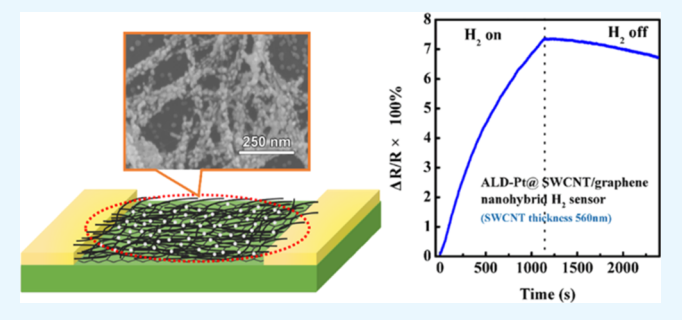
ACCESS I

Metrics & More

Article Recommendations

Supporting Information

ABSTRACT: A nanohybrid architecture composed of single-wall carbon nanotube films and graphene heterostructures (SWCNT/graphene) was developed as a three-dimensional (3D) electrode. Atomic layer deposition (ALD) was used for conformal coating of catalytic Pt nanoparticles on the 3D ALD-Pt@SWCNT/graphene nanohybrid architecture for further enhancement of H₂ sensing, taking advantage of the large sensing area and conformally coated nanostructures of the catalytic Pt. Remarkably, the H₂ response was found to be improved by 50% in the SWCNT/graphene nanohybrid, indicating that graphene provides a more efficient charge transport. The ALD-Pt further enhances the H₂ responsivity



of the 3D ALD-Pt @SWCNT/graphene nanohybrids. By coating 10 cycles of ALD-Pt on the SWCNT/graphene nanohybrid, the $\rm H_2$ response (2.77%) is approximately twice that (1.4%) of its counterpart without the ALD-Pt. By further optimizing the 3D ALD-Pt@SWCNT/graphene nanohybrids with respect to the ALD-Pt cycle numbers and SWCNT film thickness, a $\rm H_2$ responsivity as high as 7.5% was achieved on the SWCNT/graphene nanohybrid sample with a 560 nm thick SWCNT film and 50 cycles of ALD-Pt.

KEYWORDS: single-wall carbon nanotubes, platinum, atomic layer deposition, nanohybrid, hydrogen sensor

1. INTRODUCTION

Over the past 20 years, carbon nanotube (CNT)-based gas sensors have been broadly investigated for detecting various gases. Unlike classical semiconducting metal oxide gas sensors that require high operating temperatures, the CNT-based gas sensors are capable of room-temperature detection of hazardous gases, such as ammonia (NH₃)⁴ and nitrogen dioxide (NO₂). It is well known that the adsorption/desorption of electron-donating or electron-accepting gas molecules on the CNT surface can transfer electrons driven by the interactions between molecules and π electrons of CNT. This process causes a change in the resistance of the CNT, which is measured as the sensor's response.

However, prior works have demonstrated that gas sensors based on pristine CNTs suffer from poor sensitivity for many gases, for example, H₂, because of weak adsorption of H₂ molecules on the CNT surface, which results from high activation energy of the adsorption process.^{7,8} A promising approach to resolve these issues, and hence to improve the sensitivity of specific gases on CNT-based gas sensors, is to decorate catalytic metals such as gold (Au),^{9,10} silver (Ag),¹¹ platinum (Pt),¹² and palladium (Pd)^{7,8,13} on CNTs. The Pt catalysis relies on H₂ molecules adsorbing to the platinum metal, which assists in the breaking of the H–H bond.¹⁴ This process lowers the activation energy, making platinum an ideal catalyst for the hydrogen oxidation reaction. Owing to this promising catalytic property, Pt has been used to effectively

enhance the sensitivity of H_2 gas in CNT-based gas sensors. 12,15,16

Different from the previous reports that studied H₂ sensors based on Pt/CNT composites, a new three-dimensional (3D) ALD-Pt@single-wall CNT (SWCNT)/graphene nanohybrid architecture is proposed in this work to resolve the issues in the current CNT-based gas sensors. SWCNTs were selected considering that they have the largest possible aspect ratio among all the CNTs, which could possibly provide the largest sensing surface area. It should be noted that CNTs form Schottky contacts with metal electrodes (such as Au electrodes¹⁷) used in the CNT-based gas sensors, which would obstruct the charge transfer between CNTs and electrodes. In addition, the contact resistance at the CNT-CNT junctions is significantly higher than that of the CNTs, resulting in increased charge recombination and hence reduced device performance.¹⁸ By inserting a graphene sheet between the SWCNT film and metal electrodes, the SWCNT/graphene nanohybrid structure takes advantage of graphene's metallic property, extraordinary charge mobility, as well as the 3D

Received: September 2, 2020 Accepted: November 5, 2020 Published: November 17, 2020





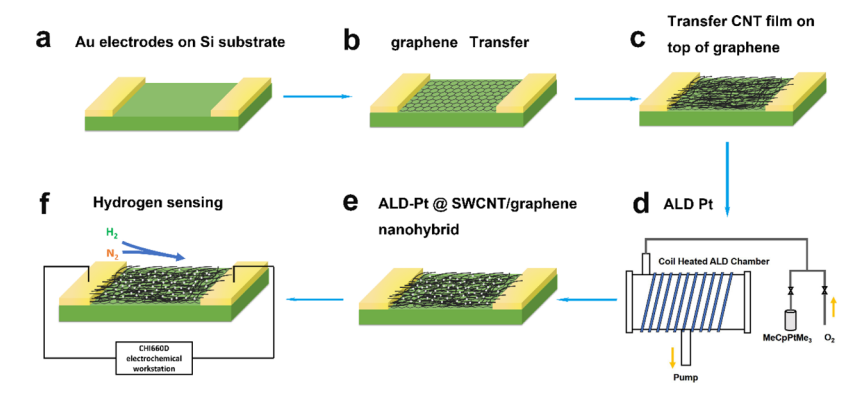


Figure 1. Schematic description of the procedure developed for fabrication of the 3D ALD-Pt@CNT/graphene nanohybrid H₂ sensors. (a) Au bar electrodes deposition; (b) graphene transfer; (c) SWCNT film transfer on graphene to form SWCNT/graphene nanohybrid; (d) ALD-Pt coating on the SWCNT/graphene nanohybrid; (e) 3D schematic structure of ALD-Pt@SWCNT/graphene nanohybrid; (f) schematic illustration of H₂ sensing measurement circuit.

porous CNT network for a large sensing area and efficient charge transfer and transport; all are important to highperformance H₂ sensors. On the other hand, the coating of the Pt catalyst on CNTs in previous reports was typically carried out using an evaporation method 12,16 or chemical reactions in solution. It should be realized that atomic layer deposition (ALD) provides the best approach for conformal coating of Pt on a nanoporous 3D electrode but unfortunately has not been applied on CNT-based H2 sensors. Conformal coating is a major advantage of ALD on a high-aspect ratio nanoporous structure, 19 and our group also studied the ALD coating of Aldoped ZnO on vertically aligned carbon nanofiber arrays previously and confirmed this.²⁰ Therefore, ALD-Pt was adopted in this work in order to obtain a conformal coating of Pt on the 3D SWCNT/graphene nanohybrid electrodes to take the most advantage of catalytic Pt. In the following, we report our experimental results. The enhancement of H₂ sensing due to ALD-Pt was confirmed by comparing Pt-coated samples with their counterparts that lacked Pt. Moreover, different ALD cycle numbers and SWCNT film thicknesses were investigated, and the optimal configuration for the SWCNT/graphene nanohybrid-based H₂ sensor was identified as a 560 nm thick SWCNT film with 50 cycles (50 c) of ALD-Pt.

2. EXPERIMENTAL SECTION

The fabrication procedure of the 3D ALD-Pt@SWCNT/graphene nanohybrid H₂ sensor is illustrated schematically in Figure 1a—e. The device fabrication involves four major steps overall, starting with the evaporation of Au bar electrodes on SiO₂/Si substrates (Figure 1a), followed by graphene transfer onto the SiO₂/Si substrates with prefabricated Au electrodes (Figure 1b). Afterward, the SWCNT film was transferred on top of the graphene (Figure 1c) in order to form the 3D SWCNT/graphene nanohybrid, followed by ALD-Pt on the SWCNT/graphene nanohybrid in a vacuum ALD chamber (Figure 1d). The completion of device fabrication is exhibited in Figure 1e. The ALD-Pt at low ALD cycle numbers results in nanoparticles (NPs) uniformly distributed on the ALD-Pt@SWCNT/graphene nanohybrid 3D architecture to be used as H₂ sensors in this work.

2.1. Sample Fabrication. 2.1.1. Au Electrode Deposition. Au electrode bars, which have the dimensions of 4 mm (length) \times 2 mm (width), were deposited on a SiO₂/Si substrate through a shadow mask using electron-beam evaporation. The distance between the neighboring Au bars is 0.3 mm, which defines the effective lateral sensing area.

2.1.2. Graphene Growth in Chemical Vapor Deposition and Transfer. Single-layer graphene was synthesized using chemical vapor

deposition (CVD) on commercial copper foils (Sigma-Aldrich) at $1000~^{\circ}\text{C}$ and then transferred onto the SiO_2/Si substrate with prefabricated Au electrodes. The details of graphene growth and transfer were reported in previous works. $^{21-23}$

2.1.3. SWCNT Film Preparation and Transfer. SWCNT films were prepared via a vacuum filtration method. SWCNT powders of 1-2 nm diameter (Shenzhen Bill Technology Development Ltd., China) and length of micrometer scale were added to DI water, together with a 1 wt % Triton X-100 surfactant. The concentration of the SWCNT suspension is 5 mg/L. The CVD SWCNTs are typically composed of roughly 1/3 metallic and 2/3 semiconducting SWCNTs by volume portions based on the mixed chirality.²⁴ For many optoelectronic applications, high-purity semiconductor SWCNTs (s-SWCNTs) are used to enable the formation of a consistent interface to generate a specific built-in electric field between s-SWCNTs and other materials. 25,26 Such purification may not be necessary in the case of the ALD-Pt@SWCNT/graphene sensors because these devices rely instead on the large effective SWCNT surface for H2 attachment and charge transport, as shown in our earlier studies comparing the purified and unpurified SWCNT films for infrared detection.² Prior to vacuum filtration, SWCNTs were dispersed by bath ultrasonication for 1 h. For the nanotube film formation, we used $0.2 \mu m$ mixed cellulose ester filter membranes in a vacuum filtration apparatus (Millipore). Care was taken when pouring the nanotube suspension into the filter funnel to avoid bubbles on the solution surface. The solution was filtered down and kept under vacuum until the film was mostly dry (~20 min). The residual surfactant left in the film was subsequently washed away with purified water. The details of SWCNT film vacuum filtration were also reported in previous works. 18,27,28 The transfer of SWCNT films was developed based on an earlier report.²⁷ The vacuum filtration-prepared membrane with the SWCNT was cut into stripes and placed (facing down) on top of substrates with deposited Au electrodes. The membrane was rinsed with DI water, and a water-absorbing piece of tissue was placed on top of the membrane. Then, a small piece of glass was used as a cover and $\sim 100 \text{ g/cm}^2$ pressure was applied from the top of the glass of cover by using a mass block. The substrate was heated at 70 °C for 1 h using a hot plate so that the SWCNT/membrane could attach tightly to the graphene/substrate. The final steps in the SWCNT film transfer were dissolving the membrane in acetone, cleaning the sample with isopropanol, and finally, drying it with N2 gas. In this study, a comparison among graphene, SWCNT films, and SWCNT/graphene nanohybrid-based H2 sensors was examined and the nanohybrid was identified as the most efficient for H2 sensing.

2.1.4. ALD of Platinum. The ALD of Pt was accomplished by using alternating exposures to MeCpPtMe₃ (Sigma-Aldrich) and oxygen at 300 °C.²⁹ During ALD, a constant flow (5 sccm) of ultrahigh-purity nitrogen (99.99%) carrier gas was passed through the reactor. The MeCpPtMe₃ precursor was heated (60 °C) to increase the vapor pressure. The reactant exposures lasted 3 s for MeCpPtMe₃ and 1 s

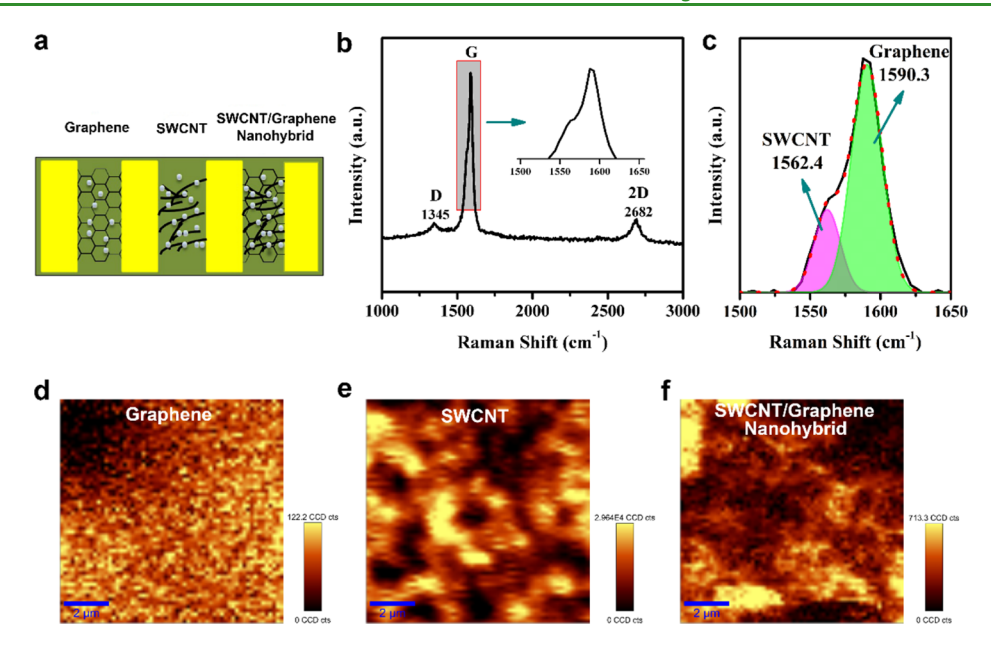


Figure 2. (a) Schematic top view of ALD-Pt@graphene, ALD-Pt@SWCNT film, and ALD-Pt@CNT/graphene nanohybrid; (b) Raman spectrum of the SWCNT/graphene nanohybrid; the inset is the enlarged G peak; (c) Gaussian fitting of G peak. Black line is the G peak extracted from (b); red dash line is the fitted G peak; purple peak represents SWCNT G mode and green peak represents graphene G mode; (d) graphene 2D peak Raman map; (e) SWCNT 2D peak Raman map; and (f) SWCNT/graphene nanohybrid 2D peak Raman map.

for oxygen, and nitrogen purges of 60 s were used between each exposure.

2.2. Sample Characterization. The thickness of the SWCNT films was measured using a KLA-Tencor P-16 stylus profilometer with a lateral resolution of 1 μm (dimension of the stylus) and a vertical resolution of 0.7 nm. The SWCNT films were cut into a ~1.5 mm wide stripe and transferred to a piece of the silicon substrate using the method discussed above. The stylus was set to move across the SWCNT film stripe width and the average thickness of the SWCNT film was obtained from the profiles of the line scans. Atomic force microscopy (AFM) images of the SWCNT/graphene nanohybrid were collected using a digital instruments multimode AFM with a nanoscope IIIa controller. All images were collected in contact mode with a scan rate of about 1.0 Hz using the same standard silicon nitride tip (Bruker, NP-S, $k \sim 0.06$ N/m). The nanohybrid was imaged in three different locations. 30 cross-sections were taken over three 2.0 μ m imes 2.0 μ m AFM images to measure the height and width (full width at half-maximum) of the CNT bundles within the nanohybrid. The dimensions have not been corrected for the effects of tip convolution. Scanning electron microscopy (SEM) images and energy-dispersive X-ray spectroscopy (EDS) spectra of the SWCNT/ graphene nanohybrid samples with different cycle numbers of ALD-Pt coating were taken on a Hitachi SU8230 ultrahigh resolution scanning electron microscope to extract the information of sample morphology and Pt element distribution. Raman spectra were measured on a WiTec alpha300 confocal micro-Raman system equipped with a piezoelectric sample stage using a 488 nm excitation laser (power ~30 mW and integration time 0.3 s). In addition, Raman maps of graphene and SWCNT signature peaks were taken to reveal the morphology of the CVD graphene and the SWCNT films in the 3D SWCNTs/ graphene electrodes. Using the 488 nm laser excitation, the spatial resolution of the Raman maps is limited to $1/2 \lambda \sim 244$ nm. In the latter, the formation of the SWCNT bundles and clusters has been reported to yield inhomogeneity in the Raman maps of SWCNT films, 30,31 which has been also confirmed in this work. This seems to agree with the large surface root-mean-square roughness (R_n) values of 2-3 μ m obtained using a profilometer (KLA-Tencor P16 with 3D porosity analysis software) on 3D ALD-Pt@SWCNT/graphene samples with 20, 50, 70, and 100 c ALD-coated Pt shown in Figure S1. While a quantitative analysis of the sample porosity remains a challenge considering the large SWCNT film thickness of hundreds of nanometers or larger and small pores (or gaps) of dimension of a few to tens of nanometers between SWCNTs or their bundles or clusters, the large surface roughness values reflect qualitatively on the porous nature of the 3D ALD-Pt@SWCNT/graphene samples. High-purity (~98%) semiconductive SWCNTs (s-SWCNTs) with a nominal diameter in the range 1.2-1.7 nm and length in the range 300 nm to 5.0 μ m (Isonanotube-S from NanoIntegris)²⁶ were also used in this study for a comparison of the physical properties of the unpurified SWCNTs used for the ALD-Pt@SWCNT/graphene 3D nanohybrid H₂ sensors in this work. It should be noted that the s-SWCNTs have a comparable morphology to that of the unpurified ones and the same vacuum filtration method was applied to make films from these two types of SWCNTs for electrical transport measurements using an Oxford cryostat with closed cycle cooling. Specifically, resistance as a function of temperature (R-T) curves was taken using a Keithley 224 current source (providing the bias currents) and a Keithley 2182 DC voltmeter (taking the voltage generated across the sample). In order to eliminate the effect of the surfactant and other molecules on the transport properties of the SWCNTs, the SWCNT films were annealed in vacuum at $<5 \times 10^{-6}$ Torr at 400 °C for 90 min.

The H₂ response and sensitivity were measured in a homemade vacuum chamber with a mixed H₂/N₂ gas flow. The ALD-Pt@ SWCNT/graphene sensors were mounted on a sample stage inside the chamber with a multipin electric feedthrough for the electric connection of the sample to external electronics. Before the measurement, the chamber was purged with a N2 flow for about an hour to remove any residual gas molecules. The concentration of H₂ was controlled by controlling the flow ratio of H2 and N2 gases using an MKS four-channel flowrate controller (MKS 946). For example, in order to obtain the 10% H₂ concentration, the H₂ and N₂ ratio was set as 20 sccm (H_2) :180 sccm (N_2) . In this work, the concentration of H_2 was varied in the range of 1–30%. Current–time (I-t) curves were recorded on the ALD-Pt@SWCNT/graphene sensors at a constant bias voltage (V) using a CH Instruments CHI660D electrochemical workstation in response to the H2 flow on and off in a vacuum chamber (illustrated in Figure 1f). The I-t curves were later converted to resistance—time (R-t) curves using the Ohm's law R =V/I, where V was set to 0.1 V in this work for responsivity calculation. The resistance of the connection between the CHI660D electrochemical workstation and device was measured to be $0.5-0.8 \Omega$, which is negligible compared to the resistance of the CNT/graphene

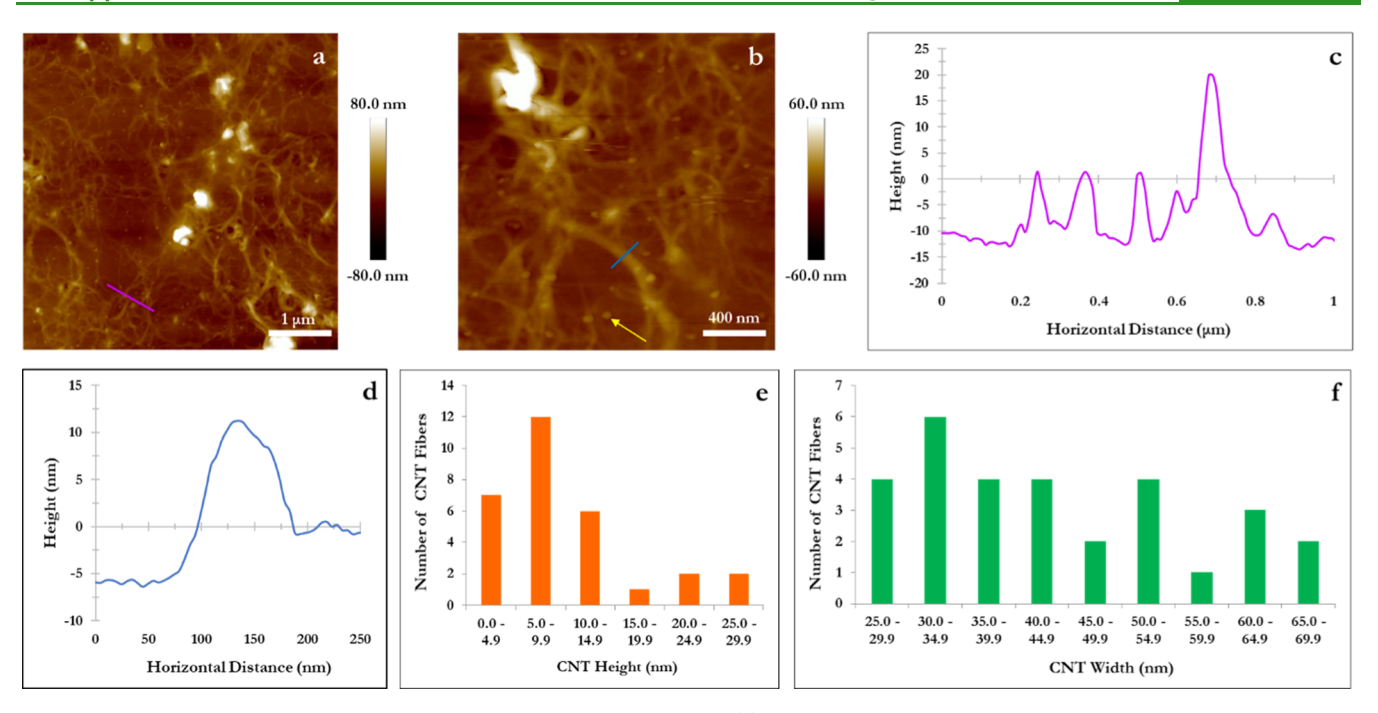


Figure 3. AFM images and cross-sections of SWCNT/graphene nanohybrid. (a) Representative 5 μ m × 5 μ m AFM image of SWCNT/graphene nanohybrid. (b) Representative 2 μ m × 2 μ m AFM image of SWCNT/graphene nanohybrid. Yellow arrow indicates example of a Pt NP. (c) Cross-sectional profile along the pink line in (a). (d) Cross-sectional profile along the blue line in (b). (e) the height distribution and (f) the width distribution of the CNT fibers within the nanohybrid, obtained from cross-sections.

hybrid $\rm H_2$ sensor typically in the range of a few hundred ohms or higher, which is important to obtaining a high signal-to-noise ratio typically in the range 100:1 or higher. The initial sensor resistance is in the range of 4.3–1500 Ω for the sensors studied in this work depending on the SWCNT thickness, ALD-Pt cycle numbers, etc. For example, the sensor resistance is the lowest at 100 c ALD-Pt coating, which is not a surprise considering an almost continuous layer of metallic Pt coated on the SWCNTs/graphene.

3. RESULTS AND DISCUSSION

Figure 2a shows three different structures compared in this work, which are ALD-Pt@graphene only, ALD-Pt@SWCNT film only, and ALD-Pt@SWCNT/graphene nanohybrid, respectively. Figure 2b shows the Raman spectrum of the SWCNT/graphene nanohybrid using a 488 nm laser and three peaks are visible. The Raman peak located at 2682 cm⁻¹ identified as the 2D mode of graphene and SWCNT, and the peak located at 1345 cm⁻¹ is the D mode. At the ~1570 cm⁻¹ peak, two subpeaks were observed. The inset of Figure 2b shows the region containing the G peak, which indicates that it is composed of two separated peaks. By doing Gaussian fitting on the G peak region as depicted in Figure 2c, two peaks centered at 1562.4 and 1590.3 cm⁻¹ are identified, which match well with the G peaks of the SWCNT film and graphene (Raman spectra are shown in Figure S2), respectively. Figure 2c-e compares the 2D peak Raman maps of graphene, the SWCNT film, and the SWCNT/graphene nanohybrid scanned on a 10 μ m \times 10 μ m area. The 2D Raman map of graphene is fairly uniform as expected. The inhomogeneity revealed in the 2D Raman map of the SWCNT film can be ascribed to the 3D porous structure of the SWCNT film anticipated from the random stacking of individual and bundles of SWCNTs during the vacuum filtration process (see Experimental Section), which can also be seen in the 2D mode Raman map of the SWCNT/graphene nanohybrid.

Figure S3a compares the normalized R-T curves of the s-SWCNTs and their unpurified counterparts in the temperature range of 200-300 K. A major difference lies in the much higher temperature dependence of the former by ~3.3 fold than that of the latter, which can be ascribed to the "shorting" of the metallic SWCNTs in the latter with a substantial volume portion. In order to quantify the volume portion of the metallic SWCNTs in the unpurified SWCNTs, the resistivity of the SWCNT films was measured as a function of the film thickness. As shown in Figure S3b, the resistivity increases monotonically with decreasing SWCNT thickness, especially below the thickness of 50–60 nm as observed previously in unpurified SWCNT films. This behavior confirms the presence of both semiconductive and metallic SWCNTs in the unpurified SWCNTs because of mixed chirality and is ascribed to the dominance of the high-resistance Schottky junctions formed between semiconductive and metallic SWCNTs over the low-resistance intertube junctions between semiconductive-semiconductive and metallic-metallic SWCNTs.³²

A summary of the AFM data collected on the SWCNT/ graphene nanohybrid is shown in Figure 3. AFM images taken at various locations on the sample showed consistent CNT bundles within the film. The image in Figure 3a is a 5 μ m \times 5 um scan at one location on the surface. The image shows a porous network of CNT bundles as well as the presence of some Pt NPs. The image in Figure 3b is 2.0 μ m \times 2.0 μ m and shows the topography in more detail, with a yellow arrow indicating a Pt NP. Again, the CNT bundles form a porous covering over the surface of the nanohybrid, as illustrated by the cross-section in Figure 3b which shows multiple CNT bundles. The separation of the bundles is quite varied but typically in the range of 50-500 nm from one bundle to the next. Cross-sectional analysis (see Figure 3d) was used to measure the dimensions of the CNT fibers. The average height was 10 ± 7 nm and the average width was 43 ± 13 nm.

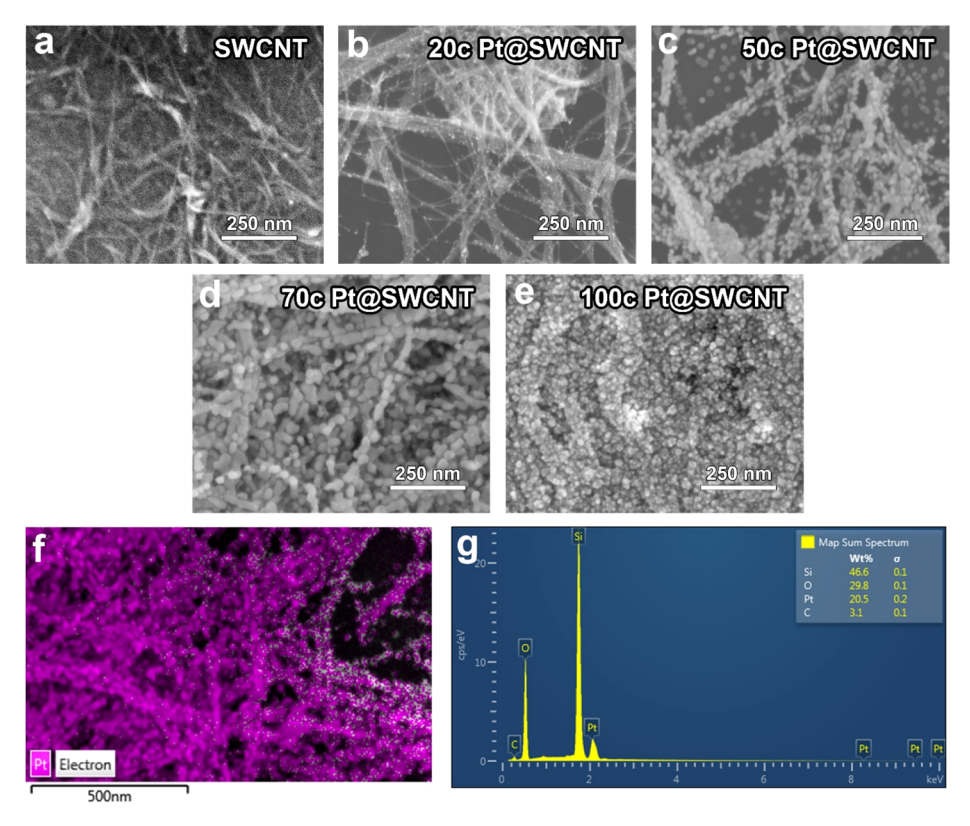


Figure 4. SEM images of (a) SWCNT/graphene nanohybrid; (b) 20 c ALD-Pt@SWCNT/graphene nanohybrid; (c) 50 c ALD-Pt@SWCNT/graphene nanohybrid; (d) 70 c ALD-Pt@SWCNT/graphene nanohybrid; (e) 100 c ALD-Pt@SWCNT/graphene nanohybrid; (f) EDS mapping and (g) EDS spectrum of 50 c Pt on SWCNT.

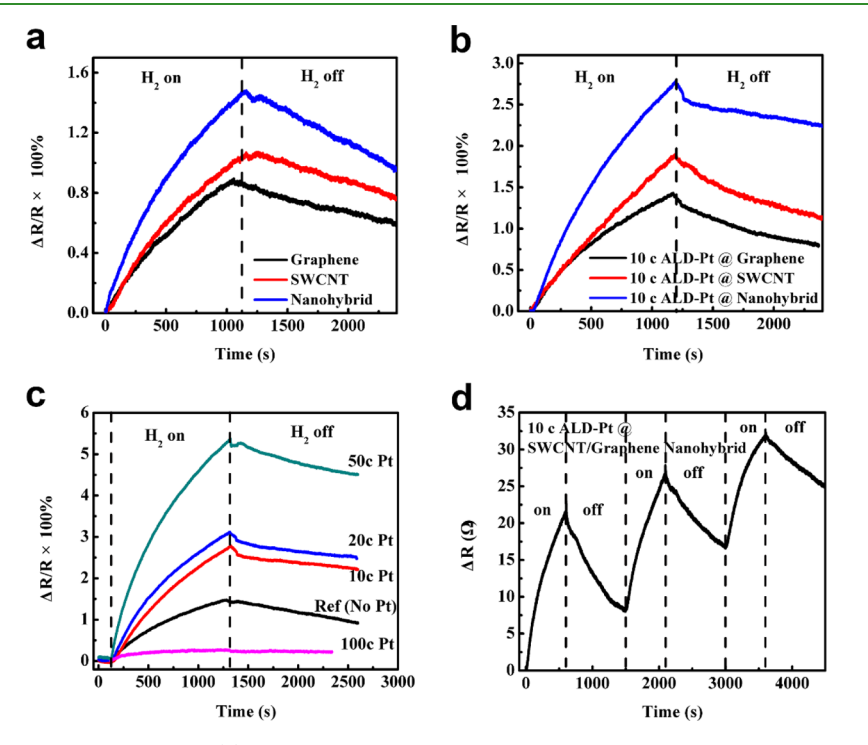


Figure 5. H_2 sensing responsivity comparisons of (a) graphene, SWCNT film and SWCNT/graphene nanohybrid sensor; and (b) 10 c ALD-Pt@ graphene, 10 c ALD-Pt@SWCNT, and 10 c ALD-Pt@SWCNT/graphene nanohybrid sensor. (c) H_2 sensing responsivity comparisons of ALD-Pt@SWCNT/graphene nanohybrid sensor that have different ALD cycle numbers; (d) 3 cycles dynamic response curve of 10 c ALD-Pt@SWCNT/graphene nanohybrid sensor. The thickness of SWCNT films is ~100 nm. For (a-c) H_2 on and off time are both 1200 s, and for (d) H_2 on time is 600 s and off time is 900 s in each cycle.

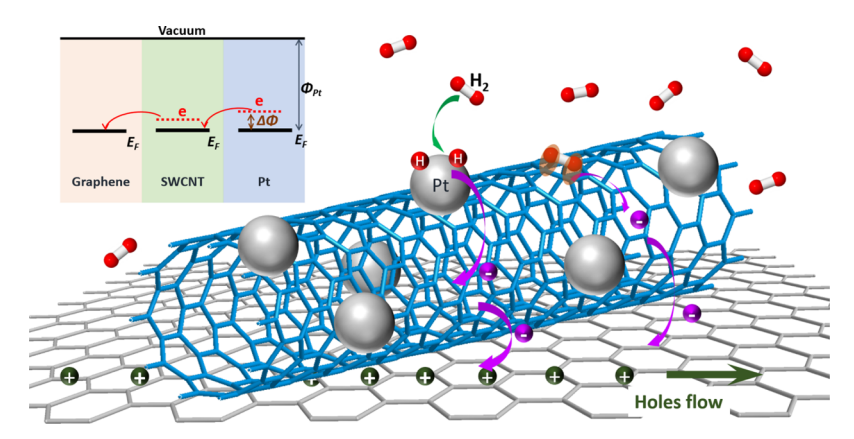


Figure 6. Schematic illustration of the hydrogen sensing mechanism on the ALD-Pt@SWCNT/graphene nanohybrid sensor.

Histograms of the height and width of the SWCNT bundles are provided in Figure 3e and f, respectively. These dimensions, as well as the topography, are consistent with the bundles of SWCNT.

Figure 4a displays the SEM morphology of the SWCNT/ graphene nanohybrid with the SWCNT film prepared via the vacuum filtration method. SWCNT networks are clearly observed. However, the diameter of each tube in Figure 4a is measured to be around 20 nm, which is 10 times larger than the normal SWCNT diameter (1-2 nm). This reveals that SWCNTs tend to assemble into bundles even after high-power ultrasonication has been performed when dispersing SWCNTs in DI water, which is consistent with the observations from AFM measurements. The bundle effect of SWCNTs was also confirmed using transmission electron microscopy in many early reports. 34-36 With confirmation of the porous scaffold of SWCNTs on the SWCNT/graphene electrodes using both AFM and SEM, it is important to understand the evolution of morphology and distribution of the catalytic ALD-Pt with increasing ALD cycle number on the scaffold because it plays a critical role in H₂ sensing in the ALD-Pt@SWCNT/graphene nanohybrid. Figure 4b-e displays the SEM images of an SWCNT/graphene nanohybrid and four ALD-Pt@SWCNT/ graphene nanohybrids with different ALD-Pt coating cycles of 20, 50, 70, and 100 c, respectively. While the highly porous morphology of SWCNTs can be clearly seen in all samples, the morphology of ALD-Pt varies systematically with increasing ALD cycle numbers. In the sample with 20 c ALD-Pt (Figure 4b), Pt NPs are uniformly and sparsely distributed surrounding the walls of SWCNTs. When the ALD-Pt cycle number is increased to 50 c, an increase in the diameter of the Pt NPs to ~20 nm and density was observed (Figure 4c). This trend continues with a further increase of the ALD-Pt cycle number to 70 c (Figure 4d), at which the Pt NP diameter has almost doubled to 30-40 nm and most SWCNTs are covered conformally with Pt NPs. At 100 c (Figure 4e), the Pt NPs seem to connect into a continuous layer and the SWCNTs are no longer visible, which is consistent with the dramatically reduced sensor resistance by 1-2 orders of magnitude to ~4.3 Ω because of the electric shorting through the Pt NP layer in this case. Figure 4f,g shows the EDS Pt mapping and EDS spectrum of the 50 c ALD-Pt@SWCNT/graphene nanohybrid, which further confirms the existence of Pt on the hybrid sample after ALD.

The H_2 sensing measurements were performed in a homemade chamber with H_2 and N_2 flow and the details are

given in the Experimental Section. The sensor responsivity is defined as the relative variation of the sensor resistance, that is, $\Delta R/R$. Figure 5a compares the H₂ sensing responsivity of devices made with graphene only, SWCNT films only, and SWCNT/graphene nanohybrids. The device made with graphene only does not show a promising responsivity to H₂ primarily because of the lack of an efficient sensing area. The device made with the SWCNT film only shows an improved responsivity compared to graphene as it has a larger sensing area that comes from its network structure. However, this improvement is limited because of the huge contact resistance in the SWCNT network. The SWCNT/graphene nanohybrid takes advantage of both the good charge transport capability of graphene and large sensing area of SWCNTs, thereby exhibiting the best H₂ sensing performance among these three samples.

After 10 c of ALD-Pt, devices of graphene, the SWCNT film, and the SWCNT/graphene nanohybrid all showed an improved H₂ sensing responsivity (Figure 5b), compared to their counterparts without Pt in Figure 5a. For example, the responsivity of the nanohybrid increased by ~97% with 10 c ALD-Pt. The enhancement in H₂ sensing is attributed to the Pt NPs coated on the SWCNTs from ALD. For the SWCNT/ graphene nanohybrid sample without Pt, the response when exposed to H₂ flow completely comes from the physisorption of H₂ molecules on SWCNTs and the consequent electron transfer from the H2 molecule to CNT because of the H2 molecule–CNT π electron interaction. However, owing to the large activation energy and poor adsorption of H2 molecules on SWCNTs, the responsivity is poor. In contrast, for the 10 c ALD-Pt@SWCNT/graphene nanohybrid sample, apart from physisorption of H₂ on the SWCNTs, Pt layers also adsorb the H₂ molecules on their surface upon exposure to H₂, and then, H₂ molecules are separated into H atoms at the outer surface of the Pt layers. This is known as a molecular chemisorption process. As illustrated in Figure 6, H atoms dissolve readily into a Pt layer, lowering its work function, which results in electron transfer from the Pt layer to the SWCNT and finally to graphene, thus increasing the resistance of SWCNTs and graphene (which are p-type in ambient). The physisorption and chemisorption work together on the ALD-Pt@SWCNT/ graphene nanohybrid sample, enhancing the H₂ sensing responsivity eventually.

Figure 5c compares the H₂ sensing responsivity of Pt@ SWCNT/graphene nanohybrid samples with different ALD cycle numbers. The device shows very poor H₂ sensing

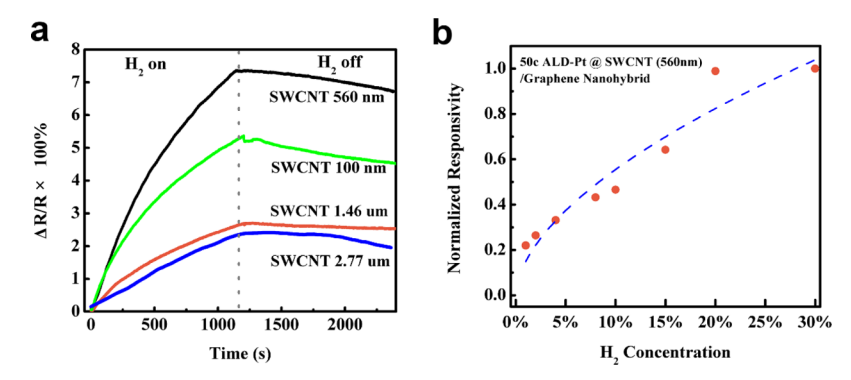


Figure 7. (a) H₂ sensing responsivity comparisons of 50 c ALD-Pt@SWCNT/graphene nanohybrid sensor that have different SWCNT film thickness; H₂ on and off time are both 1200 s; (b) normalized responsivity of 50 c ALD-Pt@SWCNT/graphene nanohybrid sensor as the function of H₂ concentration (orange dots); defining the responsivity at 30% H₂ as 1. Blue dash line is the fitting based on Langmuir adsorption model.

performance without Pt, and the responsivity increased as more cycles of ALD-Pt were coated on SWCNTs. The peak responsivity was achieved for the sample with 50 c ALD-Pt. However, when the number of ALD cycles was increased to 100 c, the responsivity of the SWCNT/graphene nanohybrid H₂ sensor dropped dramatically. This phenomenon is the result of two aspects of Pt coated on SWCNTs. As mentioned earlier, the H₂ chemisorption on Pt is the major contributor to the enhanced H₂ sensing on the Pt@SWCNT/graphene nanohybrid gas sensor. Hence, the denser the Pt particles on the SWCNT networks, the more the H2 chemisorption takes place. As shown in Figure 4b,c, Pt NPs conformally coated on the sample with 50 c ALD-Pt were much larger and denser than in the sample with 20 c ALD-Pt. In addition, the EDS spectra show that the mass fraction (wt %) of the Pt is ~20% (Figure 4f,g) in the former, almost a hundred times of the latter (~0.2%, Figure S4a,b). On the other hand, at 70 c ALD-Pt coating (Figures S4c,d), a higher Pt mass fraction of 55.6% was observed. This explains why H2 responsivity increases with more ALD-Pt cycle numbers for 10, 20, and 50 c samples. On the other hand, if the ALD cycle number is increased further, Pt NPs of high density will eventually merge into a continuous Pt film coated on the surface of SWCNT/graphene, as shown in Figure 4f, which blocks H₂ sensing area of the SWCNT network, therefore lowering the sensitivity of the 3D SWCNT/ graphene to H₂ gases. This observation indicates that the gas sensitivity of the ALD-Pt@SWCNT/graphene nanohybrid devices is a compromise of the catalytic effect of Pt and the effective surface area of the 3D SWCNT/graphene electrode. The ALD-Pt coating certainly provides advantages of uniform conformal coating of the ALD-Pt for an optimal balance of the two effects. In our experiment, 3-6 different ALD-Pt@ SWCNT/graphene devices of the same SWCNT thickness and ALD-Pt cycle number were measured in order to examine the device uniformity and reproducibility. The obtained error bars shown in Figure S5 are typically within ±20%, indicating fairly consistent uniformity and reproducibility from device to

In order to examine the repeatability of the ALD-Pt@ SWCNT/graphene nanohybrid H_2 sensors, dynamic response measurements were performed at 10% H_2 concentration. Figure S6 demonstrates that the dynamic electrical current variation is in response to H_2 gas on/off cycles and the trend is repeatable from cycle to cycle. Based on this measurement, the variation of the resistance to the H_2 gas on/off cycles can be calculated and the result is exhibited in Figure 5d. From these

measurements, it is clear that the gas sensor recovers slowly, that is, it takes a long time to return to the initial resistance after gas flow ends. Recovery is a common issue for SWCNT-based sensors because of the large activation energy between the SWCNTs and H₂ molecules, requiring higher energy or a longer time to detach from the SWCNTs. Some efforts have been made to accelerate the recovery response of SWCNT sensors by lowering the activation energy by means of UV light-induced photo desorption or with high-vacuum conditions.^{37,38}

The thickness of the SWCNT film also has a significant impact on the H₂ sensing of the ALD-Pt@SWCNT/graphene nanohybrid via affecting the charge transfer from SWCNTs to graphene. Figure 7a compares the H2 response by 50 c ALD-Pt@SWCNT/graphene nanohybrid H₂ sensors of different SWCNT film thicknesses of 100 nm, 560 nm, 1.46 μ m, and 2.77 μ m (measured at 10% H₂). All four samples were synthesized using the same SWCNT. It is clearly shown that the device with a 560 nm thick SWCNT film has the highest H_2 responsivity of $\sim 7.5\%$ among the four samples of the same architecture. The lower H₂ responsivity in the 50 c ALD-Pt@ SWCNT/graphene nanohybrid with a thinner SWCNT film may be ascribed to the smaller effective sensing area that is expected to be proportional approximately linearly to the SWCNT film thickness. When the SWCNT film thickness exceeds 560 nm, a significant decrease of the H₂ responsivity was observed. This indicates that charge transfer from the SWCNT film to graphene may become more difficult because of a longer charge transport pathway through the thicker SWCNT film despite a larger effective sensing area. The optimal thickness of SWCNT films in the ALD-Pt@SWCNT/ graphene nanohybrid sensors is a compromise between the effective sensing area and the charge transfer pathway length. Figure S7 displays the H₂ response of a 50 c Pt@SWCNT/ graphene nanohybrid sensor at different H2 concentrations in the range of 1-30%. Qualitatively, the sensor resistance increases when exposed to H2. With increasing H2 concentrations, the amplitude of the resistance variation increases monotonically. For example, the resistance change of \sim 3 Ω was observed at 1% H₂ concentration, which is about 20% of the responsivity at 30% H₂ concentration, indicating its potential in H₂ sensing at even much lower H₂ concentration. Figure 7b shows the normalized responsivity of the 50 c ALD-Pt@SWCNT/graphene nanohybrid sensor as a function of H₂ concentration (red circles) plotted from the original data in Figure S7. The blue dashed line is a fitting of the H₂

Table 1. Comparison of H₂ Sensing Performance with Early Reports on Pt Decorated CNT-Based H₂ Sensor^a

sensor platform	Pt fabrication method	H ₂ concentration (%)	H ₂ responsivity (%)	specific responsivity	refs
Super-aligned CNT film pulled from forest	evaporation	10	~7	0.7	16
MWCNT	reaction in solution	4	6.5	1.625	41
MWCNT	reaction in solution	4	8	2	15
Vertically aligned CNT	sputtering	1	1.1	1.1	42
SWCNT/graphene nanohybrid	ALD	10	7.5	0.75	this work
^a Specific responsivity is calculated by dividing H ₂ responsivity by the H ₂ concentration.					

concentration dependence of the responsivity using the Langmuir adsorption model used to explain the microscopic mechanism underlying the gas sensing on SWCNTs. 39,40 Over the H₂ concentration range from 1 to 30%, the experimental data agree well with the theory as expected. The slight deviation of the experimental data point at 20% H₂ concentration from the theoretical curve suggests that this point may be an outlier because of the data scattering. As we have discussed before, incomplete sensor recovery is a common issue for SWCNT-based gas sensors, and this slow recovery becomes more significant when measuring H2 pulses of higher H₂ concentrations as more H₂ molecules are adsorbed to the SWCNT surface. Figure S8 compares the H₂ response of two ALD-Pt@SWCNT/graphene nanohybrid H₂ sensors with 50 and 70 c of ALD-Pt. Both samples have the optimal SWCNT film thickness of ~560 nm. The reduced H₂ responsivity of the latter (70 c sample) to only 57% of the former is not a surprise considering much reduced effective sensing surface area covered by Pt and reduced catalytic activity of the Pt NPs with their increasing dimension at 70 c ALD-Pt coating, as revealed by SEM in Figure 4.

Table 1 compares the performance of the ALD-Pt@ SWCNT/graphene nanohybrid gas sensors developed in this work with some representative works of the CNT-based gas sensor decorated with Pt. Previous works typically adopted either evaporation or solution-based chemical reaction for Pt fabrication, which have disadvantages considering that these approaches consume significantly more Pt source during the fabrication while not producing a conformal Pt coating on the CNTs. In addition, impurities and reaction residue contamination of the CNT surface seem unavoidable in the solution reaction of Pt. In contrast, ALD provides the best way for conformal coating of Pt on nanoscale 3D carbon networks as discussed earlier. The best H₂ responsivity of 7.5% achieved in this work is comparable to previous works of the CNT-based gas sensor decorated with Pt based on multi-wall CNT (MWCNTs) films with surface functionalization or CNT alignments. 15,16,41,42 For CNT-based thin-film hydrogen sensors, there are two major factors relevant to the H₂ sensor performance: effective surface area and electric conductivity. When comparing SWCNTs with MWCNT films of comparable thickness, SWCNT films can ideally have a larger effective sensing area because of the larger aspect ratio (length vs diameter). However, SWCNTs have much worse dispersibility in solution than MWCNTs and thus tend to assemble into bundles easily, which reduces the effective surface area considerably of the SWCNT film. In addition, most as-made CVD SWCNTs are unpurified with about 2/3 semiconductive and 1/3 metallic SWCNTs. In contrast, MWCNTs are much more conductive because of the reduced band gap proportional to the inverse of the CNT diameter. Therefore, when comparing bundled SWCNTs with MWCNT films, they would have comparable effective surface areas. The better

conductivity in the latter would make them more favorable because the H₂ sensing signals can be more effectively transported to the electrodes. Similarly, vertically aligned CNTs have a larger sensing area than SWCNT films. However, this does not conflict with our results and the novelty of our work. By replacing SWCNTs with MWCNTs to eliminate the CNT bundling and thus enlarge the sensing area, responsivity will be enhanced further with the 3D nanohybrid device architecture.

4. CONCLUSIONS

In summary, a new 3D architecture of ALD-Pt@SWCNT/ graphene nanohybrid has been developed for H2 sensing by stacking vacuum filtration-prepared SWCNT films on the top of CVD graphene transferred onto the SiO₂/Si substrates with prefabricated electrodes, followed by ALD conformal coating of Pt NPs. This architecture has implemented two unique features, both of which are critical for improved H2 sensing performance. One is the implementation of the graphene as the signal collection component from the SWCNT films, taking the advantages of favorable band edge alignment at the interface of the SWCNT/graphene and a high charge mobility of graphene for efficient charge transfer and charge transport. The other is the implementation of the ALD for conformal coating of the catalytic Pt NPs on the 3D SWCNT/graphene electrode. These 3D ALD-Pt@SWCNT/graphene nanohybrids take advantage of not only a large effective sensor area but also the Pt's catalytic dissociation of H2 molecules in proximity of SWCNTs/graphene electrodes. Optimization of the device with respect to the SWCNT film thickness in the range of 0.1–2.8 μ m and ALD-Pt coverage with ALD cycle number varied in the range of 10-100 was carried out to obtain the best H₂ sensitivity. It has been shown that the H₂ responsivity of SWCNT/graphene nanohybrids is superior to the ones with only graphene or SWCNTs, while ALD-Pt coating on SWCNT/graphene further enhances H2 sensing owing to the catalytic property of Pt. By further optimizing the 3D ALD-Pt@SWCNT/graphene nanohybrids with respect to the ALD-Pt cycle numbers and SWCNT film thickness, H₂ responsivity as high as 7.5% was achieved on the 3D ALD-Pt@ SWCNT/graphene nanohybrids at the optimal SWCNT thickness of 560 nm and 50 cycle of ALD-Pt. It should be noted that the SWCNT films adopted in this work were selected as a proof of the concept. Replacing SWCNTs with MWCNTs could eliminate the CNT bundling and enlarge the sensing area and thus achieve further enhanced responsivity with this 3D nanohybrid device architecture. This result illustrates the ALD-Pt@CNT/graphene nanohybrid as a promising 3D architecture for high-performance sensors at low cost and scalability.

ASSOCIATED CONTENT

Supporting Information

The Supporting Information is available free of charge at https://pubs.acs.org/doi/10.1021/acsami.0c15532.

Surface morphologies obtained from profilometer; Raman spectra of graphene and SWCNT film; Comparison of purified s-SWCNT and as-prepared CVD SWCNT; EDS Pt mapping and spectra; statistical plot of responsivity; three cycles I-t dynamic response curve; dynamic response at different H_2 concentration; and H_2 response comparison of 50 c and 70 c ALD-Pt@ SWCNT/graphene nanohybrid H_2 sensor (PDF)

AUTHOR INFORMATION

Corresponding Authors

Bo Liu – Department of Physics and Astronomy, The University of Kansas, Lawrence, Kansas 66045, United States; orcid.org/0000-0003-0298-8238; Email: liubo@ku.edu

Judy Z. Wu — Department of Physics and Astronomy, The University of Kansas, Lawrence, Kansas 66045, United States; Email: jwu@ku.edu

Authors

Mohammed Alamri — Department of Physics and Astronomy, The University of Kansas, Lawrence, Kansas 66045, United States; © orcid.org/0000-0002-7473-8644

Michael Walsh — Department of Energy's National Security Campus, Kansas City, Missouri 64147, United States Jennifer L. Doolin — Department of Chemistry, The University of Kansas, Lawrence, Kansas 66045, United States Cindy L. Berrie — Department of Chemistry, The University of Kansas, Lawrence, Kansas 66045, United States; orcid.org/0000-0003-2422-8141

Complete contact information is available at: https://pubs.acs.org/10.1021/acsami.0c15532

Notes

The authors declare no competing financial interest.

ACKNOWLEDGMENTS

This research was supported by Plant Directed Research and Development funds from the Department of Energy's Kansas City National Security Campus, operated and managed by Honeywell Federal Manufacturing and Technologies, LLC under contract. The authors also acknowledge support in part by ARO contract no. W911NF-16-1-0029 and NSF contract nos. NSF-DMR-1508494, NSF-DMR-1909292, and NSF-ECCS-1809293.

REFERENCES

- (1) Sinha, N.; Ma, J.; Yeow, J. T. W. Carbon Nanotube-Based Sensors. J. Nanosci. Nanotechnol. 2006, 6, 573-590.
- (2) Zhang, T.; Mubeen, S.; Myung, N. V.; Deshusses, M. A. Recent Progress in Carbon Nanotube-Based Gas Sensors. *Nanotechnology* **2008**, *19*, 332001.
- (3) Wetchakun, K.; Samerjai, T.; Tamaekong, N.; Liewhiran, C.; Siriwong, C.; Kruefu, V.; Wisitsoraat, A.; Tuantranont, A.; Phanichphant, S. Semiconducting Metal Oxides as Sensors for Environmentally Hazardous Gases. *Sens. Actuators, B* **2011**, *160*, 580–591.

- (4) Peng, N.; Zhang, Q.; Chow, C. L.; Tan, O. K.; Marzari, N. Sensing Mechanisms for Carbon Nanotube Based NH₃ Gas Detection. *Nano Lett.* **2009**, *9*, 1626–1630.
- (5) Valentini, L.; Armentano, I.; Kenny, J. M.; Cantalini, C.; Lozzi, L.; Santucci, S. Sensors for Sub-ppm NO₂ Gas Detection Based on Carbon Nanotube Thin Films. *Appl. Phys. Lett.* **2003**, *82*, 961–963.
- (6) Wang, Y.; Yeow, J. T. W. A Review of Carbon Nanotubes-Based Gas Sensors. *J. Sens.* **2009**, 2009, 1–24.
- (7) Mubeen, S.; Zhang, T.; Yoo, B.; Deshusses, M. A.; Myung, N. V. Palladium Nanoparticles Decorated Single-Walled Carbon Nanotube Hydrogen Sensor. *J. Phys. Chem. C* **2007**, *111*, 6321–6327.
- (8) Zilli, D.; Bonelli, P. R.; Cukierman, A. L. Room Temperature Hydrogen Gas Sensor Nanocomposite Based on Pd-Decorated Multi-Walled Carbon Nanotubes Thin Films. *Sens. Actuators, B* **2011**, *157*, 169–176.
- (9) Lee, K.; Scardaci, V.; Kim, H.-Y.; Hallam, T.; Nolan, H.; Bolf, B. E.; Maltbie, G. S.; Abbott, J. E.; Duesberg, G. S. Highly Sensitive, Transparent, and Flexible Gas Sensors Based on Gold Nanoparticle Decorated Carbon Nanotubes. *Sens. Actuators, B* **2013**, *188*, 571–575.
- (10) Zanolli, Z.; Leghrib, R.; Felten, A.; Pireaux, J.-J.; Llobet, E.; Charlier, J.-C. Gas Sensing with Au-Decorated Carbon Nanotubes. *ACS Nano* **2011**, *5*, 4592–4599.
- (11) Cui, S.; Pu, H.; Mattson, E. C.; Lu, G.; Mao, S.; Weinert, M.; Hirschmugl, C. J.; Gajdardziska-Josifovska, M.; Chen, J. Ag Nanocrystal as a Promoter for Carbon Nanotube-Based Room-Temperature Gas Sensors. *Nanoscale* **2012**, *4*, 5887–5894.
- (12) Gautam, M.; Jayatissa, A. H. Adsorption Kinetics of Ammonia Sensing by Graphene Films Decorated with Platinum Nanoparticles. *J. Appl. Phys.* **2012**, *111*, 094317.
- (13) Gupta, D.; Dutta, D.; Kumar, M.; Barman, P. B.; Sarkar, C. K.; Basu, S.; Hazra, S. K. A Low Temperature Hydrogen Sensor Based on Palladium Nanoparticles. *Sens. Actuators, B* **2014**, *196*, 215–222.
- (14) Michaelides, A.; Hu, P. Catalytic Water Formation on Platinum: A First-Principles Study. *J. Am. Chem. Soc.* **2001**, *123*, 4235–4242.
- (15) Kaniyoor, A.; Ramaprabhu, S. Hybrid Carbon Nanostructured Ensembles as Chemiresistive Hydrogen Gas Sensors. *Carbon* **2011**, 49, 227–236.
- (16) Jung, D.; Han, M.; Lee, G. S. Fast-Response Room Temperature Hydrogen Gas Sensors Using Platinum-Coated Spin-Capable Carbon Nanotubes. *ACS Appl. Mater. Interfaces* **2015**, 7, 3050–3057.
- (17) Chen, H.; Xi, N.; Lai, K. W. C.; Fung, C. K. M.; Yang, R. Cnt Infrared Detectors Using Schottky Barriers and P-N Junctions Based Fets. 2009 IEEE Nanotechnology Materials and Devices Conference, 2009; pp 91–95.
- (18) Lu, R.; Xu, G.; Wu, J. Z. Effects of Thermal Annealing on Noise Property and Temperature Coefficient of Resistance of Single-Walled Carbon Nanotube Films. *Appl. Phys. Lett.* **2008**, *93*, 213101.
- (19) Elam, J. W.; George, S. M. Growth of ZnO/Al₂O₃ Alloy Films Using Atomic Layer Deposition Techniques. *Chem. Mater.* **2003**, *15*, 1020–1028.
- (20) Malek, G. A.; Brown, E.; Klankowski, S. A.; Liu, J.; Elliot, A. J.; Lu, R.; Li, J.; Wu, J. Atomic Layer Deposition of Al-Doped ZnO/Al₂O₃ Double Layers on Vertically Aligned Carbon Nanofiber Arrays. *ACS Appl. Mater. Interfaces* **2014**, *6*, 6865–6871.
- (21) Liu, B.; Gutha, R. R.; Kattel, B.; Alamri, M.; Gong, M.; Sadeghi, S. M.; Chan, W.-L.; Wu, J. Z. Using Silver Nanoparticles-Embedded Silica Metafilms as Substrates to Enhance the Performance of Perovskite Photodetectors. *ACS Appl. Mater. Interfaces* **2019**, *11*, 32301–32309.
- (22) Alamri, M.; Sakidja, R.; Goul, R.; Ghopry, S.; Wu, J. Z. Plasmonic Au Nanoparticles on 2D MoS₂/Graphene Van Der Waals Heterostructures for High-Sensitivity Surface-Enhanced Raman Spectroscopy. ACS Appl. Nano Mater. 2019, 2, 1412–1420.
- (23) Liu, B.; López-González, L. E.; Alamri, M.; Velázquez-Contrera, E. F.; Santacruz-Ortega, H.; Wu, J. Z. Cation-π Interaction Assisted Molecule Attachment and Photocarrier Transfer in Rhodamine/Graphene Heterostructures. *Adv. Mater. Interfaces* **2020**, *7*, 2000796.

- (24) Meyyappan, M. Carbon Nanotubes: Science and Applications; CRC Press, 2004.
- (25) Gong, Y.; Liu, Q.; Wilt, J. S.; Gong, M.; Ren, S.; Wu, J. Wrapping Cytochrome C around Single-Wall Carbon Nanotube: Engineered Nanohybrid Building Blocks for Infrared Detection at High Quantum Efficiency. Sci. Rep. 2015, 5, 11328.
- (26) Lu, R.; Christianson, C.; Kirkeminde, A.; Ren, S.; Wu, J. Extraordinary Photocurrent Harvesting at Type-II Heterojunction Interfaces: Toward High Detectivity Carbon Nanotube Infrared Detectors. *Nano Lett.* **2012**, *12*, 6244–6249.
- (27) Lu, R.; Li, Z.; Xu, G.; Wu, J. Z. Suspending Single-Wall Carbon Nanotube Thin Film Infrared Bolometers on Microchannels. *Appl. Phys. Lett.* **2009**, *94*, 163110.
- (28) Wu, Z.; Chen, Z.; Du, X.; Logan, J. M.; Sippel, J.; Nikolou, M.; Kamaras, K.; Reynolds, J. R.; Tanner, D. B.; Hebard, A. F.; Rinzler, A. G. Transparent, Conductive Carbon Nanotube Films. *Science* **2004**, 305, 1273–1276.
- (29) Aaltonen, T.; Ritala, M.; Sajavaara, T.; Keinonen, J.; Leskelä, M. Atomic Layer Deposition of Platinum Thin Films. *Chem. Mater.* **2003**, *15*, 1924–1928.
- (30) Dresselhaus, M. S.; Dresselhaus, G.; Saito, R.; Jorio, A. Raman Spectroscopy of Carbon Nanotubes. *Phys. Rep.* **2005**, 409, 47–99.
- (31) Saito, R.; Hofmann, M.; Dresselhaus, G.; Jorio, A.; Dresselhaus, M. S. Raman Spectroscopy of Graphene and Carbon Nanotubes. *Adv. Phys.* **2011**, *60*, 413–550.
- (32) Bekyarova, E.; Itkis, M. E.; Cabrera, N.; Zhao, B.; Yu, A.; Gao, J.; Haddon, R. C. Electronic Properties of Single-Walled Carbon Nanotube Networks. *J. Am. Chem. Soc.* **2005**, *127*, 5990–5995.
- (33) Lu, R.; Kamal, R.; Wu, J. Z. A Comparative Study of 1/f Noise and Temperature Coefficient of Resistance in Multiwall and Single-Wall Carbon Nanotube Bolometers. *Nanotechnology* **2011**, 22, 265503.
- (34) Hou, P.-X.; Yu, B.; Su, Y.; Shi, C.; Zhang, L.-L.; Liu, C.; Li, S.; Du, J.-H.; Cheng, H.-M. Double-Wall Carbon Nanotube Transparent Conductive Films with Excellent Performance. *J. Mater. Chem. A* **2014**, *2*, 1159–1164.
- (35) Markiewicz, K. H.; Wilczewska, A. Z.; Chernyaeva, O.; Winkler, K. Ring-Opening Reactions of Epoxidized SWCNT with Nucleophilic Agents: A Convenient Way for Sidewall Functionalization. *New J. Chem.* **2014**, *38*, 2670–2678.
- (36) Mishra, P.; Harsh; Islam, S. S. Trace Level Ammonia Sensing by SWCNTs (Network/Film) Based Resistive Sensor Using a Simple Approach in Sensor Development and Design. *Int. Nano Lett.* **2013**, *3*, 46.
- (37) Rajaputra, S.; Mangu, R.; Clore, P.; Qian, D.; Andrews, R.; Singh, V. P. Multi-Walled Carbon Nanotube Arrays for Gas Sensing Applications. *Nanotechnology* **2008**, *19*, 345502.
- (38) Snow, E. S.; Perkins, F. K.; Robinson, J. A. Chemical Vapor Detection Using Single-Walled Carbon Nanotubes. *Chem. Soc. Rev.* **2006**, *35*, 790–798.
- (39) Bannov, A. G.; Jašek, O.; Prášek, J.; Buršík, J.; Zajíčková, L. Enhanced Ammonia Adsorption on Directly Deposited Nanofibrous Carbon Films. *J. Sens.* **2018**, *2018*, *1*–14.
- (40) Kokabu, T.; Inoue, S.; Matsumura, Y. Estimation of Adsorption Energy for Water Molecules on a Multi-Walled Carbon Nanotube Thin Film by Measuring Electric Resistance. *AIP Adv.* **2016**, *6*, 115212.
- (41) Kumar, M. K.; Ramaprabhu, S. Nanostructured Pt Functionlized Multiwalled Carbon Nanotube Based Hydrogen Sensor. *J. Phys. Chem. B* **2006**, *110*, 11291–11298.
- (42) Penza, M.; Rossi, R.; Alvisi, M.; Signore, M. A.; Cassano, G.; Dimaio, D.; Pentassuglia, R.; Piscopiello, E.; Serra, E.; Falconieri, M. Characterization of Metal-Modified and Vertically-Aligned Carbon Nanotube Films for Functionally Enhanced Gas Sensor Applications. *Thin Solid Films* **2009**, *517*, 6211–6216.